techniques give good consistency for concentrations down to 5%.

Conclusions

From the data of Table IV we conclude that eq 1 can be used to describe specimens for which the ratio M_w(PSD)/M_w(PSH) lies between 0.32 and 1.94. The expression cannot be used for larger differences in the physical properties of the marked and unmarked molecules. This is demonstrated by the rapid deterioration of $\langle R_g^2 \rangle_w^{1/2}$ shown in Table IV for ratios of M_w(PSD)/M_w(PSH) greater than 2.0. The derivation of eq 1 is based on a minimal dependence on x in the various scattering functions (eq 2a–c) and an agreement at a mismatch level as large as 3.0 is perhaps surprising.

Since eq 1 fails for large weight differences, the examination of such systems must, for the present, be studied by conventional low-concentration measurements. Our attempt to do so shows a significantly lower $\langle R_g^2 \rangle_w^{1/2}$ than should be expected on any physical grounds. It is possible that the concentration used was too high to ignore interference between marked chains.

The fact that for both low- and high-concentration samples the $\langle R_g^2 \rangle_w^{1/2}$'s obtained for large mismatch, for example, $n_D > 9n_H$, are very much lower than expected for matched molecular weights cannot be explained on any physical basis known to us. A change in the behavior of a long chain in the presence of smaller chains was earlier reported by Kirste for poly(dimethylsiloxane)[13] but the change in $\langle R_g^2 \rangle_w^{1/2}$ is in a direction opposite to the present data. There is evident need to explore such systems further.

Acknowledgment. We are grateful to D. F. R. Mildner and O. A. Pringle for their assistance on the MURR-SANS spectrometer.

References and Notes

(1) Williams, C. E.; Nierlich, M.; Cotton, J. P.; Jannink, G.; Boue, F.; Daoud, M.; Farnoux, B.; Picot, C.; de Gennes, P. G.; Rinaudo, M.; Moan, M.; Wolff, C. *J. Polym. Sci., Polym. Lett. Ed.* **1979**, *17*, 379.
(2) Ackasu, A. Z.; Summerfield, G. C.; Jahshan, S. N.; Han, C. C.; Kim, C. Y.; Yu, H. *J. Polym. Sci., Polym. Phys. Ed.* **1980**, *18*, 863.
(3) Tangari, C.; Summerfield, G. C.; King, J. S.; Berliner, R.; Mildner, D. F. R. *Macromolecules* **1980**, *13*, 1546.
(4) Wignall, G. D.; Hendricks, R. W.; Koehler, W. C.; Lin, J. S.; Wai, M. P.; Thomas, E. L.; Stein, R. S. *Polymer* **1981**, *22*, 886.
(5) Summerfield, G. C. *J. Polym. Sci., Polym. Phys. Ed.* **1981**, *19*, 1011.
(6) The PSH material and the PSD material with M_w = 87 000 were supplied by Pressure Chemical Co. through L. Rosen. The PSD materials with M_w = 64 000 and M_w = 194 000 were prepared and characterized by Dr. L. Fetters, The University of Akron.
(7) Mildner, D. F. R.; Berliner, R.; Pringle, O. A.; King, J. S. *J. Appl. Crystallogr.*, in press.
(8) Debye, P. *J. Phys. Colloid Chem.* **1947**, *51*, 18.
(9) Flory, P. *J. Chem. Phys.* **1949**, *17*, 303.
(10) Greschner, G. S. *Makromol. Chem.* **1973**, *170*, 203.
(11) Altgelt, K.; Schulz, G. V. *Makromol. Chem.* **1960**, *36*, 209.
(12) de Gennes, P. G. "Scaling Concepts in Polymer Physics"; Cornell University Press: Ithaca, N.Y., 1979.
(13) Kirste, R. G.; Lehnen, B. R. *Makromol. Chem.* **1976**, *177*, 1137.

Small-Angle X-ray Scattering Study of Perfluorinated Ionomer Membranes. 2. Models for Ionic Scattering Maximum

Mineo Fujimura, Takeji Hashimoto,* and Hiromichi Kawai

Department of Polymer Chemistry, Faculty of Engineering, Kyoto University, Kyoto 606, Japan. *Received April 23, 1981*

ABSTRACT: The origin of the "ionic scattering maximum", attributed to the presence of ionic clusters in perfluorinated ionomer membranes, was studied by computer simulations of the observed scattering profiles and of their variations with swelling and deformation of the membranes on the basis of two models: (i) the two-phase model, in which the ionic clusters (ion-rich regions) are dispersed in the matrix of the intermediate ionic phase composed of fluorocarbon chains and nonclustered ions (single ions, small multiplets), and (ii) the core–shell model, in which the ionic cluster (i.e., ion-rich core) is surrounded by the fluorocarbon phase (i.e., ion-poor shell), the core–shell particle itself being dispersed in the matrix of the intermediate ionic phase. A clear distinction between the models turns out to be generally difficult. That is, the general aspects of the variation of the scattering profiles with swelling and deformation can be described in terms of either of the two models, and thus the distinction between the models requires quantitative investigations of the scattering profiles in terms of shifts of the peak position and height and so on. However, the swelling behavior, especially the result that the microscopic degree of swelling as determined by small-angle X-ray scattering is much larger than the macroscopic degree of swelling, clearly supports the core–shell model, the "short-range order distance" of which gives rise to the ionic scattering maximum. The deformation behavior also tends to support the core–shell model, although it is less conclusive than the swelling behavior.

I. Introduction

In part 1[1] of this series we studied the small-angle X-ray scattering (SAXS) behavior of perfluorinated, carboxylated, or sulfonated ionomer membranes that were chemically modified from a series of Nafion[2] membranes having different equivalent weights (EW, i.e., the weight of polymer that will neutralize 1 equiv of base). We found two SAXS maxima: one at small s (=(2 sin θ)/λ, 2θ and λ being the scattering angle and the wavelength of the X-rays used in our experiments, 1.54 Å), which arises from an interlamellar spacing, and the other at large s, which is designated as the "*ionic scattering*" maximum and which originates from the presence of ionic clusters, i.e., the region rich in ionic sites.

The size of the ionic clusters is experimentally found to depend on the kinds of cations and anions, the equivalent weight, the amount of water present in the membranes, and the temperature.[1] The dependencies of the cluster size on these physicochemical factors are shown to be predictable, at least in principle, in terms of the theory pro-

0024-9297/82/2215-0136$01.25/0

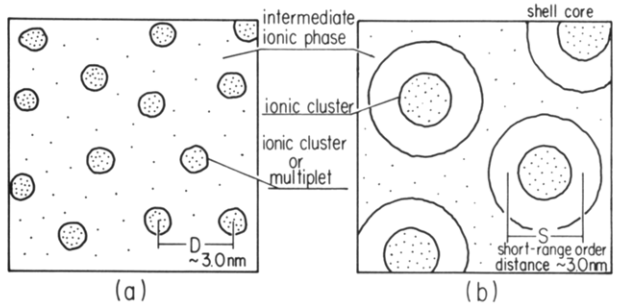

Figure 1. Two models describing the ionic SAXS maximum for perfluorinated ionomer membranes: (a) two-phase model, for which the ionic scattering peak arises from interparticle interference; (b) core–shell model, for which the ionic scattering peak arises from intraparticle interference. The crystalline region is ignored in the schematic diagram for simplicity. The dots indicate ionic sites.

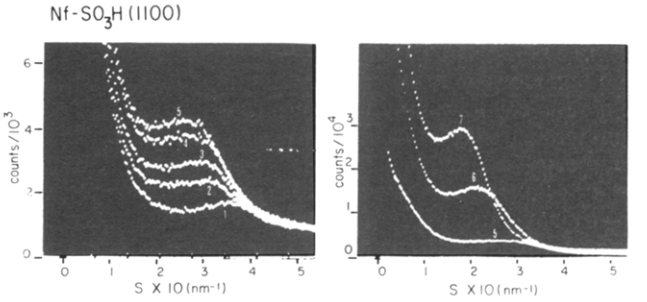

Figure 2. Typical oscilloscope displays of SAXS profiles obtained with the position-sensitive X-ray detector. A series of profiles was obtained for the sulfonic acid membranes having 1100 EW with different amounts of water uptake: curve 1, standard-state dry; curves 2–6, soaked, respectively, in 20, 15, 10, 5, and 0 wt % aqueous solutions of sodium chloride at room temperature; curve 7, standard-state swollen. The amount of water uptake increases in the order of curves 1–7.

posed by Eisenberg.[3] We experimentally found that the cluster size is controlled essentially by two counterbalancing physical factors: the thermodynamic work required for polymer coil deformation in order to form the clusters and the electrostatic energy released upon cluster collapse through ion–dipole interactions.

We compared the two models on the spatial organization of the ionic sites in order to account for the variations of SAXS profiles with equivalent weight, temperature, amount of water present in the membranes, and types of anions and cations. The two models are nothing other than those that have been proposed to describe the ionic scattering maximum of hydrocarbon-based ionomer membranes such as polyethylene, polystyrene, polybutadiene, etc. (see Figure 1): (i) the *two-phase model* proposed by Cooper et al.[4] and (ii) the *core–shell model* proposed by Stein, MacKnight, and co-workers.[5,12] We showed that these two models nearly equally well describe qualitative aspects of the ionic scattering maximum of the Nafion-based ionomer membranes.[1] It should be noted that the schematic diagrams showing the models in Figure 1 ignore the crystalline region, for simplicity, and emphasize existence of the ionic clusters.

For the two-phase model the scattering maximum should essentially arise from *interparticle interference*, reflecting a regular *intercluster distance* (*D*). On the other hand, for the core–shell model the scattering maximum should essentially arise from an *intraparticle interference* of the core–shell particle, reflecting a "*short-range order distance*" (*S*) associated with size of the core and shell[5] (see Figure 1). In this paper we shall attempt to distinguish the models by computer simulation of the scattering profiles. For this purpose we quantitatively studied the swelling behavior of the membranes (section II-1) as well as their deformation behavior (section II-2).

The swelling behaviors are contrasted with those predicted by the swollen core–shell model and the two-phase model (see section IV-1). Experimental evidence that the microscopic degree of swelling as determined by SAXS is much larger than the macroscopic degree of swelling (see section II-1) definitely favors the core–shell model. The deformation behaviors (section II-2) were analyzed on the basis of ellipsoidally deformed core–shell particles and on the basis of Debye hard spheres[6] subjected to uniaxial deformation in such a way that the spatial distribution of the scattering center is given by an affine deformation (i.e., deformed two-phase model) (see section IV-2). Both the core–shell model and the two-phase model give rise to similar effects on the scattering patterns and can describe experimental profiles at small deformation. The microscopic deformation (draw ratio λ_d) as determined from the SAXS turns out to be slightly smaller than the macroscopic draw ratio λ_B. This evidence also gives support in favor of the core–shell model rather than the two-phase model, although it is less conclusive than the swelling experiment (section II-2). Needless to say, both models are good for describing the membranes in the absence of an applied electric field.

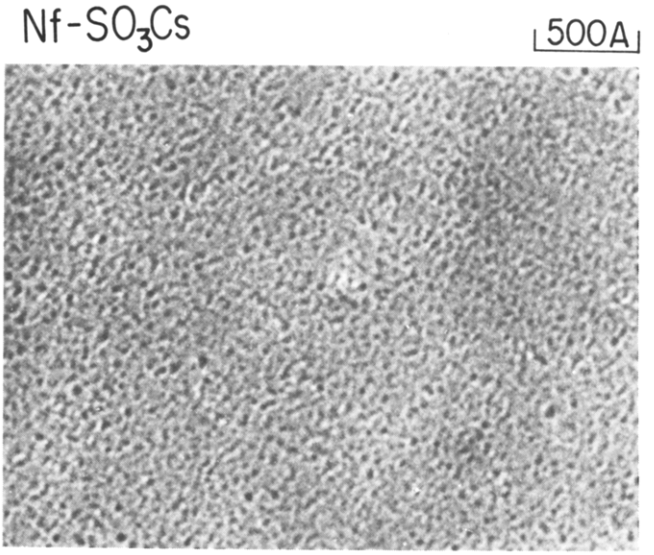

Figure 3. Typical transmission electron micrograph of an ultrathin section (about 60 nm) of perfluorinated ionomer membrane with cesium sulfonate groups having 1100 EW.

II. Experimental Results

The test specimens used in these studies and the SAXS techniques are described in detail in part 1[1] and will not be repeated here. All the SAXS profiles were obtained with a linear position-sensitive detector (PSD).

Figure 2 shows typical oscilloscope displays of the SAXS profiles obtained by the PSD. A series of profiles was obtained for sulfonic acid membranes (1100 EW) having different amounts of water uptake. The water uptake increases in the order of the curves numbered 1–7, the detailed analysis of which will be given in section II-1. Curve 1 was obtained for "standard-state dry" membranes, i.e., for membranes that were dried at 107 °C for 18 h, in a vacuum oven. The curves numbered 2–6 were obtained, respectively, for membranes soaked in 20, 15, 10, 5, and 0 wt % aqueous solutions of sodium chloride, and curve 7 was obtained for "standard-state swollen" membranes,

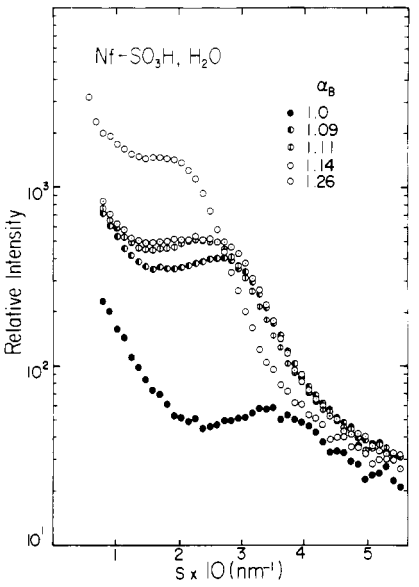

Figure 4. Variations of the ionic SAXS profiles with water uptake for membranes with sulfonic acid groups having 1100 EW. $s = (2 \sin \theta)/\lambda$ (θ is half the scattering angle).

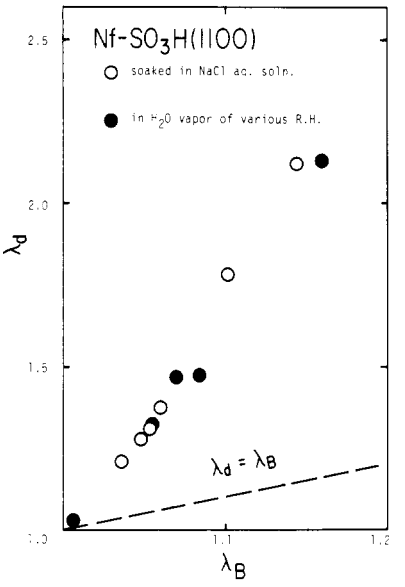

Figure 5. Relation between the microscopic degree of swelling, λ_d, and the macroscopic degree of swelling, λ_B, for membranes with sulfonic acid groups having 1100 EW. $\lambda_d = d/d_0$ (d and d_0 are the Bragg spacings as measured by the SAXS technique under the wet and dry states, respectively), and $\lambda_B = l/l_0$ (l and l_0 are the linear dimensions of the membranes as measured by a microscope or by mass change under the wet and dry states). The data points marked by open circles were obtained by soaking the membranes in aqueous solutions of sodium chloride of varying concentrations, while those marked by solid circles were obtained by changing the relative humidity of the membranes.

i.e., for membranes that were soaked in boiling water for a 0.5 h.

Figure 3 presents a typical transmission electron micrograph of an ultrathin section (about 60 nm) of perfluorinated ionomer membrane with cesium sulfonate groups having 1100 EW. The micrograph exhibits dark particles of a few nanometers in diameter, which may be domains rich in cesium atoms. During electron microscopic observations the dark particles were observed to grow into larger size. The growth may be due to crystallization of cesium atoms caused by the interaction of the electron beam with matter. A similar observation was reported by Hashimoto et al.[7] for crystallization of thorium atoms in the field of an electron beam. Thus the microscopic observation suggests existence of ionic clusters of sizes comparable to those found from the SAXS studies.[1]

1. Swelling Behavior. We investigated the swelling behavior of membranes with sulfonic acid groups or those with sodium sulfonate groups (both having 1100 EW) with water. We contrasted the microscopic degree of swelling, α_M, as measured by the SAXS technique with the macroscopic degree of swelling, α_B, as measured from changes of macroscopic dimensions of the membranes or from changes of mass of the membranes.

Figure 4 shows the SAXS profiles measured as a function of the amount of water uptake by membranes having sulfonic acid groups with 1100 EW. The parameter α_B is the ratio of weight of the wet membrane to that of the dry membrane. The α_B value of 1.26 is the equilibrium swelling degree that can be attained in the standard state, i.e., the value of the standard-state swelling that was obtained after boiling the membrane for 0.5 h in water. Values of α_B from 1.09 to 1.14 were obtained by varying the relative humidity of the membranes at room temperature. The SAXS profiles were corrected for nonuniformity of the detector sensitivity, finite spatial resolution of the detector, slit-width and slit-length smearings, and absorption, the details of which were described elsewhere.[8,9]

With an increased amount of water uptake, the scattering maximum shifts toward smaller angles or smaller s, and scattering intensity increases. The increase of intensity occurs as a consequence of increasing electron density difference between the clusters and their surrounding medium. The electron density of the clusters is decreased to a much greater extent than that of the medium as a consequence of a preferential water uptake by the clusters.[1] The shift of the scattering maximum is due either to increased intercluster distance (D), according to the two-phase model, or to increasing short-range order distance (S), according to the core–shell model[1] (see Figure 1).

From the peak position of the SAXS (s_{max} or $2\theta_{max}$) shown in Figure 4 we estimated the spacing d as a function of α_B using Bragg's equation

$$s_{max} = (2 \sin \theta_{max})/\lambda = 1/d \qquad \text{(II-1)}$$

and a linear expansion ratio λ_d of the microscopic spacing, defined by

$$\lambda_d = d/d_0 \qquad \text{(II-2)}$$

where d_0 is the spacing under the dry state. The microscopic expansion ratio of the dimension λ_d due to water uptake is then compared to the macroscopic change of the dimension λ_B

$$\lambda_B = l/l_0 \qquad \text{(II-3)}$$

where l and l_0 are the dimensions of the membrane under the wet and dry states, respectively. Figure 5 shows a comparison between λ_B and λ_d (solid circles), the broken line corresponding to the case $\lambda_B = \lambda_d$. The result indicates that λ_d is much larger than λ_B, which strongly favors the core–shell model. That is, preferential water uptake by clusters results in increased short-range order distances (S), with the microscopic expansion ratio being much larger than the macroscopic expansion ratio. If the expansion of the SAXS spacing d is due to the expansion of intercluster distances (D), then λ_d should be nearly equal to λ_B, provided that the clusters are distributed, more or less, uniformly in space.

One can also control the amount of water uptake by soaking the membranes in aqueous solutions of sodium chloride of varying concentrations. The amount of water

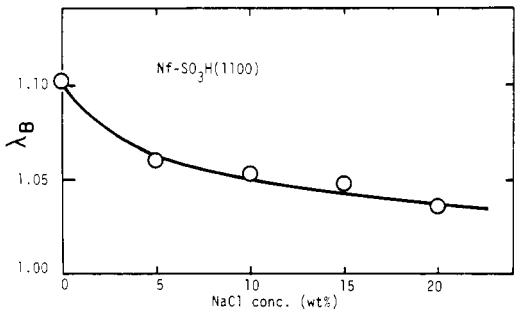

Figure 6. Swelling ratio $\lambda_B = l/l_0$ as a function of concentration of sodium chloride in water for membranes with sulfonic acid groups having 1100 EW.

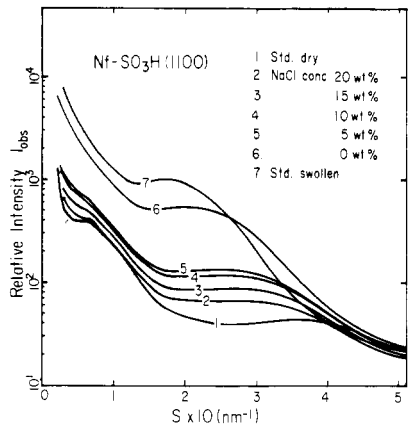

Figure 7. Variation of the ionic SAXS profiles with concentration of sodium chloride in water for membranes with sulfonic acid groups having 1100 EW.

uptake decreases and consequently $\lambda_B = l/l_0$ decreases with increasing concentration of sodium chloride as shown in Figure 6. The SAXS profiles vary with changes in sodium chloride concentration as shown in Figure 7. That is, with increasing water uptake, the SAXS maximum shifts toward smaller s and the maximum intensity increases, the general trend of which is in accord with that shown in Figure 4. The change in microscopic expansion ratio λ_d with water uptake is again contrasted with the macroscopic expansion of the linear dimension, λ_B, the results of which were also included in Figure 5 (open circles). Again the change of λ_d is seen to be much larger than that of λ_B.

The relationship between λ_d and λ_B was also explored for membranes having sodium sulfonate groups (1100 EW). The results are shown in Figure 8, in which the water uptake in the membranes is controlled either by changing the relative humidity of the membranes (solid circles) or by soaking the membranes in aqueous sodium chloride solutions (open circles). Again it is found that λ_d is much larger than λ_B. Therefore this relationship between λ_d and λ_B seems to hold in general, which strongly supports the core–shell model rather than the two-phase model.

In order to rationalize the two-phase model in terms of the experimental observations on λ_d vs. λ_B, one must consider a model in which clusters are distributed inhomogeneously in space, that is, a model which has regions rich in clusters and regions poor in clusters. Thus water is preferentially taken up by the regions rich in clusters, giving rise to λ_d greater than λ_B. However, this model does not seem to be very probable.

2. Deformation Behavior. The SAXS profiles were measured as a function of draw ratio λ_B of membranes subjected to uniaxial stretching. The stretching direction was rotated with respect to the horizontally mounted PSD in order to measure the SAXS profiles as a function of

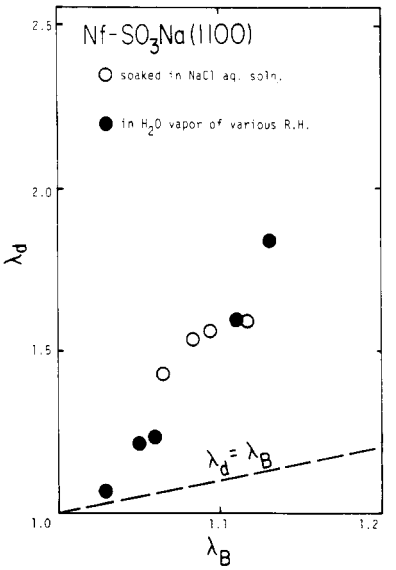

Figure 8. Relationship between the macroscopic degree of swelling, λ_B, for membranes with sodium sulfonate groups having 1100 EW. The meaning of the data marked by open and closed circles is the same as in Figure 5.

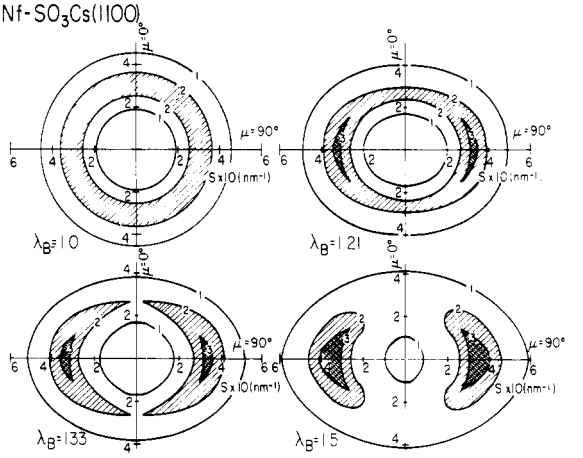

Figure 9. Contour patterns of the ionic SAXS intensity distributions as a function of stretching ratio λ_B. The stretching direction (SD) is vertical.

azimuthal angle (μ). The angle μ is the angle between the stretching direction and the scanning plane. In order to avoid complications arising from anisotropic slit smearing of the scattering profiles, inherent to systems having an anisotropic scattered intensity distribution, we used a circular focal spot image, collimation of the incident beam with a pair of circular pinholes, and a height-limiting slit in front of the positive-sensitive detector[9] to produce a nearly isotropic slit-weighting function. The experiments were conducted for cesium sulfonate membranes having 1100 EW to establish the origin of the ionic scattering maximum.

Figure 9 represents contour patterns of the SAXS intensity distribution associated with the ionic clusters as a function of the stretching ratio λ_B. With increasing λ_B, the pattern becomes elliptical, with the major axis of the ellipse oriented along equator (i.e., $\mu = 90°$). The ionic scattering maximum at the meridian ($\mu = 0°$) decays in intensity and shifts toward smaller angles, while that at the equator increases and shifts toward larger angles. The changes of the SAXS profiles at a given μ with λ_B are shown more quantitatively in Figures 10 and 11.

Figure 10 shows the SAXS profiles at the initial stage of deformation ($\lambda_B = 1.11$). It is clearly seen that the

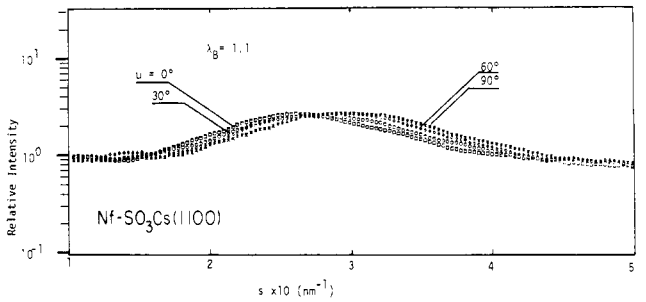

Figure 10. SAXS intensity distributions at various azimuthal angles μ at the initial stage of deformation, λ_B = 1.11.

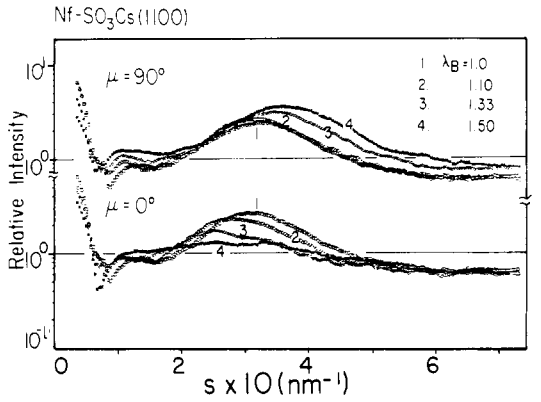

Figure 11. SAXS intensity distributions at μ = 0° and 90° as a function of λ_B for cesium sulfonate membranes having 1100 EW.

meridional SAXS maximum shifts toward smaller scattering angles s (the smaller the μ, the larger the shift), whereas the equatorial SAXS maximum shifts toward larger s (the larger the μ, the larger the shift), the intensity level of the scattering maximum remaining about the same for all μ. As shown in Figure 11 upon further increase of λ_B, the equatorial maximum tends to be enhanced and shifted further toward larger s values, while the meridional maximum tends to be depressed and shifted further toward smaller s. Therefore the intensity level of the scattering maximum becomes dependent upon μ at large deformation.

From the scattering angle giving rise to the maximum intensity, s_{max}, we estimated the spacing d as a function of λ_B and μ by using eq II-1. From the d values, the extension (or draw) ratio λ_d was calculated from eq II-2 as a function of λ_B and μ, where d and d_0 are the spacings under the deformed and undeformed states, respectively. The results are plotted in Figure 12 for a number of μ as a function of λ_B.

As seen in Figure 12, the microscopic draw ratio λ_d as measured from the Bragg spacing increases with λ_B at the polar zone (e.g., μ = 0 and 30°) and decreases at the equatorial zone (e.g., μ = 60 and 90°). However, the variations of λ_d with λ_B are less than those predicted from the affine deformation under constant volume (cf. the four broken curves in Figure 12). How can we interpret the result in terms of the two models?

If the membranes have a two-phase structure and the ionic scattering maximum arises from an intercluster interference effect, the microscopic deformation evaluated from $\lambda_d(\mu)$ should be close to the macroscopic deformation. The experimental result that measured λ_d's are less than those predicted from the affine deformation can be explained only if the deformation of the membranes is very inhomogeneous.

If the membranes have a core–shell structure, the microscopic deformation λ_d is associated with the deformation

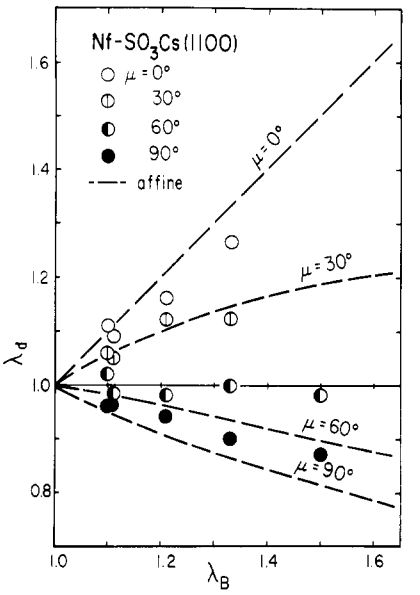

Figure 12. Relationship between the microscopic extension ratio λ_d at various μ and the macroscopic extension ratio λ_B for the Nf-SO_3Cs membranes stretched uniaxially. The broken curves correspond to the changes of d at μ = 0, 30, 60, and 90° that are predicted from an affine deformation under constant volume.

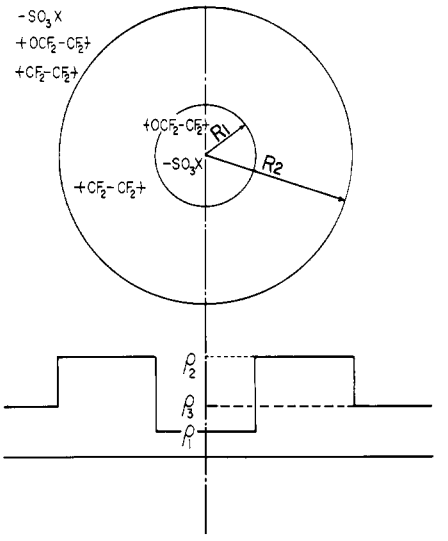

Figure 13. Isolated core–shell particle with a core radius R_1 and an outer shell radius R_2 and its electron density profile across the particle, the densities ρ_1, ρ_2, and ρ_3 being chosen as parameters.

of the short-range order distance S. The deviation of the measured values of λ_d from the predicted values (broken lines) would then reflect that deformation of the core–shell particle is less than the bulk deformation. This may occur if the core–shell particle is more rigid than the matrix phase. If the deformation of the membranes is homogeneous, as it appears, the experimental result favors the core–shell model, although the evidence is less conclusive than the evidence from the swelling experiments.

In section IV-2 these experimental results will be compared with the calculated SAXS profiles based on (i) deformed, ellipsoidal core–shell particles or (ii) an assembly of Debye hard spheres (i.e., clusters) subjected to deformation in order to distinguish the models.

III. Simulation of the Ionic Scattering Curves: Theoretical Background

We shall try to predict the changes of the ionic SAXS profiles with water uptake and deformation based upon the two models.

1. Core–Shell Model. Figure 13 represents an isolated core–shell particle with a core radius R_1 and an outer shell radius R_2. The particles are assumed to be randomly dispersed in a matrix of the intermediate ionic phase so that interparticle interference is negligible. The electron densities of the core, shell, and matrix are ρ_1, ρ_2, and ρ_3, respectively.

Average scattered intensity from the core–shell particles, $I_{cs}(q)$, is given by

$$I_{cs}(q) = \int dR_1\, P_r(R_1) I(q;R_1,R_2) / \int dR_1\, P_r(R_1) \qquad \text{(III-1)}$$

where $P_r(R_1)$ is the distribution function for the particle size. We assume here that R_2/R_1 = constant and that

$$P_r(R_1) = \exp\{(R_1 - \bar{R}_1)^2/2\sigma^2\} \qquad \text{(III-2)}$$

where $\bar{R}_1$ is the mean value of R_1 and σ^2 is the variance. $I(q;R_1,R_2)$ is the scattering from an isolated core–shell particle, which is given by

$$I(q;R_1,R_2) = I_e|F(q;R_1,R_2)|^2$$

$$F(q;R_1,R_2) = V_1(\rho_1 - \rho_2)\Phi(u_1) + V_2(\rho_2 - \rho_3)\Phi(u_2) \qquad \text{(III-3)}$$

$$\Phi(u_i) = 3(\sin(u_i) - u_i \cos(u_i))/u_i^3 \qquad \text{(III-4)}$$

$$u_i = qR_i \qquad q = 2\pi s \qquad V_i = 4\pi R_i^3/3$$

Thus the relative scattering intensity profile depends on R_1, R_2, $(\rho_1 - \rho_2)/(\rho_2 - \rho_3)$, and σ.

The changes of the scattering profiles with water uptake may be interpreted as a result of changing those parameters described above. Here, we consider a case where the volume of the shell is independent of the amount of water uptake; i.e.

$$R_{2w}^3 - R_{1w}^3 = R_2^3 - R_1^3 \qquad \text{(III-5)}$$

where R_{2w} and R_{1w} are the values corresponding to R_2 and R_1 in the wet state, respectively.

Upon stretching the membranes we assumed that a core–shell particle is deformed affinely with a constant volume into an ellipsoidal core–shell. The scattered intensity from the deformed core–shell particle is given by simply replacing u_i in eq III-4 by u_i^*

$$u_i^* = u_i \lambda_B^{-1/2}\{1 + (\nu^2 - 1)\cos^2\theta \cos^2\mu\}^{1/2} \qquad \text{(III-6)}$$

where ν is the axial ratio of the ellipsoidal particle, given by

$$\nu^2 = \lambda_B^3 \qquad \text{(III-7)}$$

and μ is the azimuthal angle ($\mu = 0°$ specifies the intensity distribution along the meridian, i.e., parallel to the stretching direction).

2. Two-Phase Model. The scattering from an assembly of ionic clusters in the undeformed state may be described by the Zernicke–Prins theory[10,11] for simple liquids.

$$I_{TP}(q) = I_e N\left\{\langle|F|^2\rangle - \frac{1}{v}|\langle F\rangle|^2 \int dD\, [1 - P(D)]\, \frac{\sin(qD)}{qD} 4\pi D^2\right\} \qquad \text{(III-8)}$$

where F is the structure amplitude of a cluster of radius R and is given by

$$F(q,R) = V(\rho_c - \rho_m)\Phi(u) \qquad u = qR \qquad \text{(III-9)}$$

for a cluster of radius R and electron density ρ_c embedded in a matrix of electron density ρ_m. V is the volume of the cluster. $\langle|F|^2\rangle$ or $\langle F\rangle$ designates an average of $|F|^2$ or F with respect to the distributions of size and scattering power, i.e., ρ_c. We assume that the scattering power ρ_c is the same for all particles and that only the size R is distributed, according to eq III-2. The function $P(\mathbf{D})\, d\mathbf{D}$ is a radial distribution function for the scattering centers, i.e., the conditional probability that, given a particle center in volume element $d\mathbf{D}_i$, one can find another particle center in volume element $d\mathbf{D}$ separated by a displacement vector $\mathbf{D}$. N is the number of clusters in the assembly and v is the volume occupied by a particle. Therefore for the two-phase model, the ionic scattering maximum is essentially described by the characteristic distance in the function $P(D)$.

In this work we shall treat the simplest case (Debye hard spheres)[6] where

$$P(D) = 1 \qquad \text{for } D \geq 2R$$

$$P(D) = 0 \qquad \text{for } D < 2R \qquad \text{(III-10)}$$

R is the radius of a sphere (i.e., a cluster). For isotropic systems with monodisperse cluster size, eq III-8 is simply given by

$$I_{TP}(q)/I_eN = |F(u)|^2\left\{1 - \frac{8V}{v}\Phi(2u)\right\} \qquad \text{(III-11)}$$

where $\Phi(2u)$ is given by eq III-4 and V/v is the volume fraction of the particle in the assembly. If there is a size distribution for the cluster, $P(D)$ may be modified as $P'(D)$

$$P'(D) = \int_0^\infty d(2R)\, P(D) W(2R) \qquad \text{(III-12)}$$

where $P(D)$ is given by eq III-10 and $W(2R)$ is the probability of finding the two particles whose radii R_1 and R_2 sum up to $2R$. The function $W(2R)$ may be given by

$$W(2R) = \int_0^\infty dR_1\, P_r(R_1) P_r(2R - R_1) \equiv P_r * P_r(2R) \qquad \text{(III-13)}$$

where P_r is the distribution function for the size of the clusters, which may be given by eq III-2 for a Gaussian distribution. Thus the scattering intensity can be calculated by inserting eq III-12 into eq III-8.

The variation of the SAXS profiles with water uptake can be described in terms of the variation of the parameters R, $\rho_c - \rho_m$, and σ.

We shall also describe the variation of the SAXS profiles with the deformation based on the Debye hard-sphere model subjected to the deformation. In this "*oriented, hard-spheroidal particle*" model, we assume that the vectors connecting the scattering centers are affinely deformed with constant volume. There are no interactions between the particles other than the impenetrability of the particles as invoked in the Debye hard spheres. The particles themselves may be affinely deformed.

For the systems with oriented hard ellipsoids, the scattering intensity $I_{TP}^d(\mathbf{q})$ is given by, similar to eq III-11,

$$I_{TP}^d(\mathbf{q})/I_eN = |F(u_p)|^2\left\{1 - \frac{8V}{v}\Phi(2u_d)\right\} \qquad \text{(III-14)}$$

where the size and shape of the clusters are assumed to be monodisperse for simplicity. The functions F and Φ are given by eq III-9 and III-4, respectively. In the case when both interparticle distances and particles themselves are affinely deformed under constant volume, it follows that

$$u_p = u_d = u\lambda_B^{-1/2}[1 + (\lambda_B^3 - 1)\cos^2\theta \cos^2\mu]^{1/2} \qquad \text{(III-15)}$$

where u is given by eq III-9, R being the radius of the clusters in the undeformed state. The details of the derivation will be given in the Appendix. Thus SAXS profiles can be calculated as a function of λ_B.

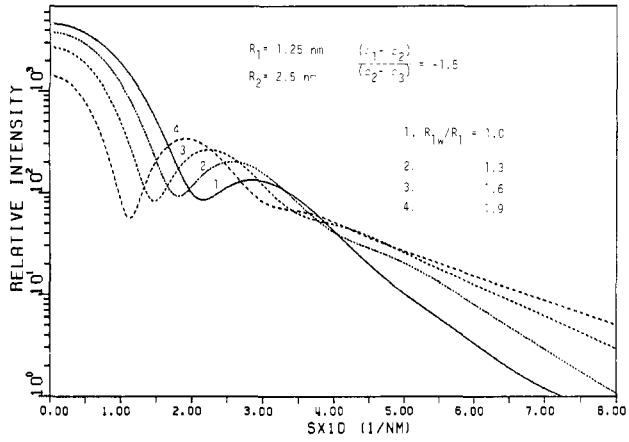

Figure 14. Effect of increasing the core radius, as a manifestation of preferential water uptake by the ionic clusters, on the calculated SAXS profiles. R_1 = 1.25 nm, R_2 = 1.5 nm, and $(\rho_1 - \rho_2)/(\rho_2 - \rho_3) = -1.5$. The core radius was increased from R_1 to R_{1w}, the ratio R_{1w}/R_1 being changed from 1.0 to 1.9.

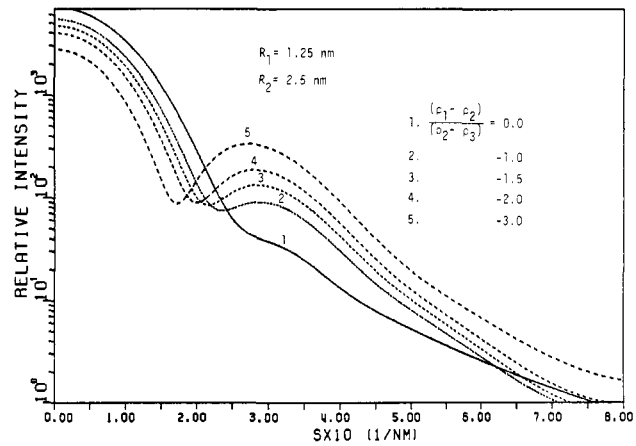

Figure 15. Effect of varying the electron density of the core, as a manifestation of preferential water uptake by the ionic clusters, on the SAXS profiles, with other parameters constant. R_1 = 1.25 nm, R_2 = 2.5 nm, and $\rho_2 - \rho_3$ = 1.0 (relative unit). A series of profiles, numbered 1–5, was calculated for $\rho_1 - \rho_2$ = 0.0, −1.0, −1.5, −2.0, and −3.0, respectively.

IV. Results and Discussion. Simulation of the Ionic Scattering Profiles and Comparison with Experimental Profiles

1. Swelling Behavior. Figures 14 and 15 show effects of the swelling on the SAXS profiles calculated for the core–shell model. Figure 14 shows the effect of increased core radius, which reflects preferential water uptake by the ionic clusters, with $(\rho_1 - \rho_2)/(\rho_2 - \rho_3)$ unchanged. The profiles are calculated for a given set of parameters, R_1 = 1.25 nm, R_2 = 2.5 nm, $(\rho_1 - \rho_2)/(\rho_2 - \rho_3) = -1.5$. The parameters R_1 and R_2 are the radii of the inner core and outer shell in the dry state, which are estimated by fitting the calculated and measured profiles. There exist some uncertainties in the values of R_1 and R_2. However, we are not interested in a rigorous estimation of the parameters; instead we are more interested in examining whether the model can describe the general trends of the variations of the SAXS with water uptake. For membranes with sulfonic acid groups, the density of the core, ρ_1, should be lower than that of the shell, ρ_2 (as found in section II-1). The density of the medium, ρ_3, should be such that $\rho_1 < \rho_3 < \rho_2$ and $\rho_2 - \rho_3 < \rho_2 - \rho_1$. Thus we assumed that $(\rho_1 - \rho_2)/(\rho_2 - \rho_3) = -1.5$, since we are only interested in relative intensity distributions or variations of them with water uptake. Of course, the expansion of the core with water uptake also involves the change of the shell size, as given by eq III-5. In calculating the profile, we set $\sigma/R_1 = 0.2$ for the size distribution in order to avoid a higher order scattering maximum from appearing. With increasing the core size the ionic scattering appearing at $s \sim 3 \times 10^{-1}$ nm^{-1} shifts toward smaller s and its intensity is enhanced.

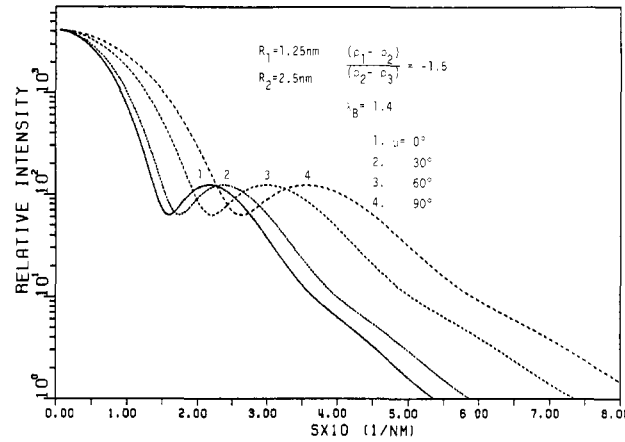

Figure 16. Calculated SAXS profiles at various azimuthal angles μ for an oriented, ellipsoidal core–shell particle with a draw ratio λ_B = 1.4.

Figure 15 shows the effect of varying the density of the core while keeping the other parameters constant as in Figure 14 (i.e., R_1 = 1.25 nm, R_2 = 2.5 nm, ρ_2 = 1.0, ρ_3 = 0.0, and σ/R_1 = 0.2). The curves numbered 5–1 are obtained for ρ_1 = −2.0, −1.0, −0.5, 0.0, and 1.0 or for $(\rho_1 - \rho_2)/(\rho_2 - \rho_3)$ = −3.0, −2.0, −1.5, −1.0, and 0.0, respectively.[14] It is seen that the intensity maximum at $s \simeq 3 \times 10^{-1}$ nm^{-1} tends to increase as the density of the core is decreased. The general trend that the ionic peak intensity increases and the peak position shifts toward smaller s as a result of preferential water uptake by the cluster core is in good agreement with that found in the experimental results on sulfonic acid membranes. The SAXS profiles for the other types of membranes can also be described by the core–shell model.

The general trend in the variation of the ionic scattering profiles with water uptake of the membranes may be also described by the two-phase model, i.e., by the simple Debye hard-spheres model. That is, an increase of cluster (or multiplet) size due to water uptake increases the average interparticle distance, resulting in a shift of the peak position to smaller angles. The water uptake tends to decrease the electron density of the cluster and therefore enhances the electron density difference between the clusters and the medium (for the sulfonic acid membranes), resulting in an increased peak intensity. Consequently, distinction between the two models must be made in terms of the amount of peak shift and intensity change. However, the experimental observation showing that the amount of peak shift is much larger than that expected from the change in bulk dimensions definitely favors the core–shell model over the two-phase model as discussed in section II-1 (Figures 5 and 8).

2. Deformation Behavior. Figure 16 shows the SAXS profiles for an isolated, oriented, ellipsoidal core–shell particle with a draw ratio λ_B = 1.4 at various azimuthal angles μ. In calculating the SAXS profiles in Figures 16 and 17, we used the same set of the parameters as for Figures 14 and 15: R_1 = 1.25 nm, R_2 = 2.5 nm, $(\rho_1 - \rho_2)/(\rho_2 - \rho_3) = -1.5$ and σ/R_1 = 0.2. The parameters $(\rho_1 - \rho_2)/(\rho_2 - \rho_3)$ and σ/R_1 are assumed to be independent of λ_B. It is shown that the ionic SAXS profiles are dependent upon

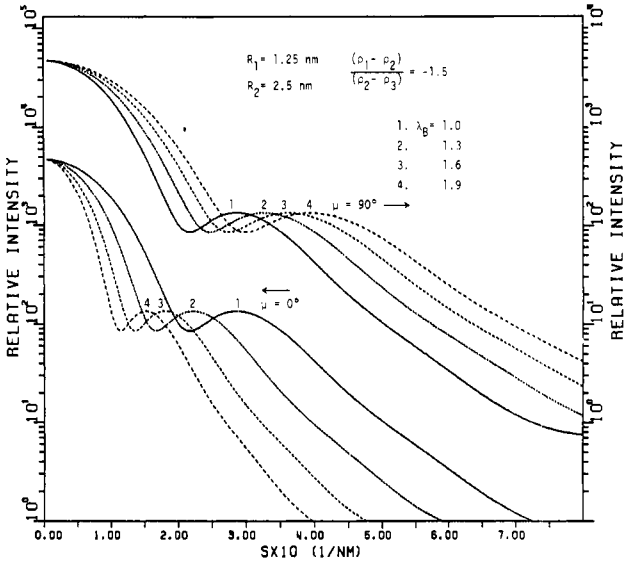

Figure 17. Calculated SAXS profiles at $\mu = 0$ and 90° as a function of λ_B for an oriented, ellipsoidal core–shell particle.

μ; the meridional maximum ($\mu = 0°$) shifts toward smaller s, but the equatorial maximum ($\mu = 90°$) shifts toward larger s, while the maximum intensity level itself is independent of μ. Figure 17 shows SAXS profiles at $\mu = 0$ and 90° as a function of λ_B. It is seen that with increasing λ_B, the meridional SAXS maximum shifts toward smaller s, but the equatorial maximum shifts toward larger s, resulting in a greater μ dependence of the SAXS distribution. The intensity level of the scattering maximum itself, however, is independent of λ_B and μ. The calculated results in Figure 17 are obtained for the deformation under constant volume. Therefore the intensity level is independent of λ_B.

The results obtained in Figures 16 and 17 are in good agreement with the experimental results at very small deformation (e.g., Figure 10). At large deformation the calculated profiles deviate from those experimentally found in that the peak intensity of the measured profiles is a function of μ, while that of the calculated profiles is independent of μ. The deviations may be partially explained in terms of an inhomogeneous deformation of the core–shell particles at large deformation that involves a destruction of the core–shell structure in the polar part, i.e., the region parallel to the stretching direction, to result in a loss of short-range order distance S.

The inhomogeneous deformation should involve a peak broadening and a loss of peak intensity at $\mu = 0°$ with λ_B, as found experimentally (Figure 11). However, it is not able to account for the observed increase of the peak intensity at $\mu = 90°$ with λ_B. This discrepancy may be attributed to an oversimplified assumption of the deformation under constant volume. Volume dilatation occurs with deformation of most of polymeric materials, except for ideal rubbers. Thus it may be conceivable that the volume of the core–shell particles may also increase with deformation, which results in increased scattered intensity with λ_B since absolute scattered intensity is proportional to the square of the particle volume. Consequently, the variation of the observed profiles with λ_B may be qualitatively described on the basis of the ellipsoidal core–shell particles with a volume dilatation and with an inhomogeneously deformed region in the polar part.[13] The inhomogeneity, leading to a loss of short-range order distance, should increase with λ_B.

Figure 18 shows the change of the ionic SAXS profiles with λ_B which are calculated on the basis of the oriented

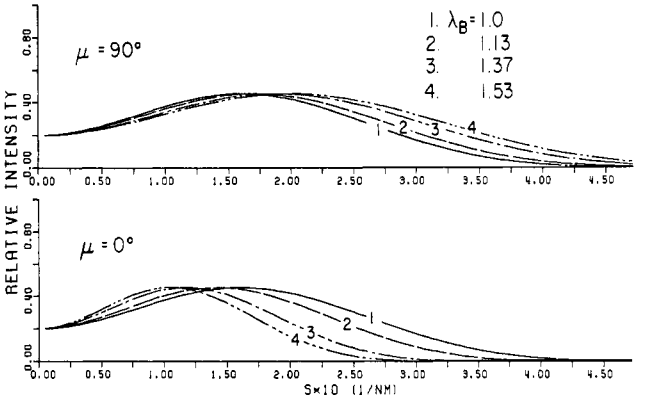

Figure 18. Calculated SAXS profiles at $\mu = 0$ and 90° as a function of λ_B for oriented, deformed Debye hard particles. $V/v = 0.1$ and $R = 1.5$ nm (radius of spheres in the undeformed state).

hard particles. Here we calculated the scattered intensity from eq III-14 and III-15. That is, we assume, for simplicity, that both particles and interparticle distances in the Debye hard spheres are affinely deformed under constant volume. The profiles are calculated for R (radius of the sphere in the undeformed state) = 1.5 nm and $V/v = 0.1$ as a function of λ_B at $\mu = 0$ and 90°.

The change of the profiles with λ_B for the deformed hard particles is quite similar to that for the deformed core–shell particles. That is, the scattering maximum at $\mu = 0°$ shifts toward smaller s but that at $\mu = 90°$ shifts toward larger s with increasing λ_B. The intensity level of the scattering maximum, however, is independent of λ_B and μ. Consequently, the variations of the observed scattering profiles with deformation can be qualitatively described by either one of the models. The distinction between the models must be made in terms of quantitative difference in the amount of the peak shifts and peak intensity change. The experimental observation that the microscopic strain λ_d is less than the macroscopic strain λ_B, however, tends to support the core–shell model as discussed in section II-2.

V. Concluding Remarks

We have explored the SAXS arising from ionic clusters existing in perfluorinated ionomer membranes. We investigated variations of the SAXS profiles with water uptake and uniaxial stretching of the membranes in order to distinguish the two possible models, i.e., the two-phase model and the core–shell model, which have been proposed to account for the ionic scattering maximum from hydrocarbon-based ionomer membranes. As for the two-phase model, we studied the scattering from Debye hard spheres (for the unoriented dry and swollen membranes) and oriented Debye hard ellipsoids (for the stretched membranes). As for the core–shell model, we studied the scattering from a spherical core–shell particle (for the unoriented dry and swollen membranes) and an oriented, ellipsoidal core–shell particle (for the stretched membranes).

The two models turned out to give similar effects on the variation of the profiles with water uptake and deformation and qualitatively account for general features of the experimental observations. Therefore distinction between the two models must be made in terms of a quantitative investigation of the peak shift and the peak intensity change with water uptake and deformation. The experimental observations that the macroscopic degree of swelling as determined from the SAXS curves is much less than the microscopic degree of swelling and that the microscopic draw ratio (again as determined from the SAXS curves) is slightly less than the macroscopic draw ratio

seem to favor the core–shell model rather than the two-phase model.

Acknowledgment. We are indebted to Drs. N. Kawasaki, T. Hashimoto, and M. Fukuda of Toyo Soda Manufacturing Co., Ltd., Yamaguchi-ken, Japan, for providing the perfluorinated ionomer membranes.

Appendix. Scattering Formula for Debye Hard Spheres Subjected to Uniaxial Deformation

The Zernicke–Prins formula for an oriented system may be given by

$$I_{TP}^{d}(\mathbf{q})/I_eN = \langle|F|^2\rangle + \frac{1}{v}|\langle F\rangle|^2 \int d\mathbf{D}'\, P'(\mathbf{D}') \exp[-i\mathbf{q}\cdot\mathbf{D}'] \quad \text{(A-1)}$$

where the primed quantities are those corresponding to the deformed state. We assume an affine deformation under constant volume, which gives

$$P'(\mathbf{D}')\, d\mathbf{D}' = P(\mathbf{D})\, d\mathbf{D} \quad \text{(A-2)}$$

where the unprimed quantities are those corresponding to the undeformed state.

$$\mathbf{D}' = D'[\sin(\alpha')\cos(\Omega')\mathbf{i} + \sin(\alpha')\sin(\Omega')\mathbf{j} + \cos(\alpha')\mathbf{k}] \quad \text{(A-3)}$$

$$\mathbf{q} = (2\pi/\lambda)[(1 - \cos 2\theta)\mathbf{i} - (\sin 2\theta \sin\mu)\mathbf{j} - (\sin 2\theta \cos\mu)\mathbf{k}] \quad \text{(A-4)}$$

$\mathbf{i}$, $\mathbf{j}$, and $\mathbf{k}$ are the unit vectors along the three Cartesian coordinate axes, $\mathbf{i}$ and $\mathbf{k}$ being set parallel to the propagation direction of the incident beam and the stretching direction, respectively. D', α', and Ω' in eq A-3 can be related to D, α, and Ω in the undeformed state from the affine deformation hypothesis

$$D' = D[\lambda_2^2 \sin^2\alpha + \lambda_3^2 \cos^2\alpha]^{1/2}$$
$$\cos\alpha' = \lambda_3 \cos\alpha[\lambda_2^2 \sin^2\alpha + \lambda_3^2 \cos^2\alpha]^{-1/2} \quad \text{(A-5)}$$
$$\cos\Omega' = \cos\Omega$$

λ_3 and λ_2 are the draw ratios along the stretching direction and the directions normal to the stretching axis, respectively. With eq A-2 to A-5, eq A-1 can be rewritten in terms of the unprimed variables only

$$I_{TP}^{d}(\mathbf{q})/I_eN = \langle|F|^2\rangle + \frac{|\langle F\rangle|^2}{v(qA^{1/2})^3}\int_0^{2\pi} d\Omega \int_0^{\pi} d\alpha \sin\alpha \int_0^{\infty} dt\, t^2 P(D) \times \cos[t\{\cos\delta \sin\alpha \sin(\Omega - \gamma) + \sin\delta \cos\alpha\}] \quad \text{(A-6)}$$

where

$$\cos\delta \sin\gamma \equiv \lambda_2 A^{-1/2}$$
$$\cos\delta \cos\gamma \equiv \lambda_2 A^{-1/2} \cos\theta \sin\mu$$
$$\sin\delta \equiv \lambda_3 A^{-1/2} \cos\theta \cos\mu \quad \text{(A-7)}$$
$$A \equiv \lambda_2^2 \sin^2\theta + \cos^2\theta(\lambda_2^2 \sin^2\mu + \lambda_3^2 \cos^2\mu)$$
$$t \equiv A^{1/2} qD$$

Upon integrating (A-6) with respect to Ω and α, one obtains

$$I_{TP}^{d}(\mathbf{q})/I_eN = \langle|F|^2\rangle + \frac{4\pi}{v}\frac{|\langle F\rangle|^2}{f(q,\mu)}\int_0^{\infty} dD\, DP(D) \sin[f(q,\mu)D] \quad \text{(A-8)}$$

where

$$f(q,\mu) = q[\lambda_2^2 \sin^2\theta + \cos^2\theta(\lambda_2^2 \sin^2\mu + \lambda_3^2 \cos^2\mu)]^{1/2} \quad \text{(A-9)}$$

Equation A-8 is a generalized scattering formula for oriented systems, which is reduced to the Zernicke–Prins formula (i.e., eq. III-8 for an unoriented system having $\lambda_2 = \lambda_3 = 1$. If there is no size distribution for the clusters and they have radius R

$$P(D) = 1 \quad \text{for } D \geq 2R$$
$$P(D) = 0 \quad \text{for } D < 2R \quad \text{(A-10)}$$

and if the clusters themselves also affinely deformed with constant volume, we obtain

$$I_{TP}^{d}(\mathbf{q})/I_eN = |F(u_d)|^2\left\{1 - \frac{8V}{v}\Phi(2u_d)\right\} \quad \text{(A-11)}$$

where

$$u_d = u\lambda_B^{-1/2}[1 + (\lambda_B^3 - 1)\cos^2\theta \cos^2\mu]^{1/2} \quad \text{(A-12)}$$

u is given by eq III-9, $\lambda_3 = \lambda_B$, and $\lambda_2 = \lambda_B^{-1/2}$.

References and Notes

(1) Fujimura, M.; Hashimoto, T.; Kawai, H. *Macromolecules* **1981**, *14*, 1309.
(2) Registered trademark of E. I. du Pont de Nemours & Co. Inc. for its perfluorinated sulfonic acid products.
(3) Eisenberg, A. *Macromolecules* **1970**, *3*, 147.
(4) Marx, C. L.; Caulfield, D. F.; Cooper, S. L. *Macromolecules* **1973**, *6*, 344.
(5) MacKnight, W. J.; Taggart, W. P.; Stein, R. S. *J. Polym. Sci., Part C* **1974**, *45*, 113.
(6) Debye, P. *Phys. Z.* **1927**, *28*, 135.
(7) Hashimoto, H. "Analytical Electron Microscopy, Report of a Specialist Workshop", Aug 1976, Cornell University, Ithaca, N.Y.
(8) Fujimura, M.; Hashimoto, T.; Kawai, H. *Mem. Fac. Eng. Kyoto Univ.* **1981**, *43* (2), 224.
(9) Hashimoto, T.; Suehiro, S.; Shibayama, M.; Saijo, K.; Kawai, H. *Polym. J.* **1981**, *13*, 501.
(10) Zernicke, F.; Prins, J. A. *Z. Phys.* **1927**, *41*, 184.
(11) Debye, P.; Menke, H. *Phys. Z.* **1930**, *31*, 797.
(12) Roche, E. J.; Stein, R. S.; Russell, T. P.; MacKnight, W. J. *J. Polym. Sci., Polym. Phys. Ed.* **1980**, *18*, 1497.
(13) The change of the profiles may also be explained in terms of orientation and deformation of cylindrical or lamellar core–shell particles as in the work of Roche et al.[12].
(14) Curve 1 in Figure 15 corresponds to the scattering curve for simple spheres of average radius $R_2 = 2.5$ nm with a size distribution characterized by $\sigma/R_2 = 0.2$. While a simple sphere exhibits only a broad and weak scattering maximum, as shown by curve 1, the core–shell particles with the same size distribution have an enhanced scattering maximum, as shown by curves 2–5, due to the short-range order distance S.
(15) The anisotropy of the film specimens as measured by light scattering and birefringence was negligible or, at least, small, and the swelling of the films specimens was isotropic.